International Journal of Multiphase Flow 35 (2009) 580–596

Contents lists available at ScienceDirect

International Journal of Multiphase Flow

journal homepage: www.elsevier.com/locate/ijmulflow

Algebraic turbulence modeling in adiabatic gas–liquid annular two-phase flow

Andrea Cioncolini [a,1], John R. Thome [a,*], Carlo Lombardi [b,2]

[a] Heat and Mass Transfer Laboratory, École Polytechnique Fédérale de Lausanne, EPFL-STI-IGM-LTCM, Station 9, 1015 Lausanne, Switzerland
[b] Department of Nuclear Engineering, Politecnico di Milano, via Ponzio 34/3, 20133 Milano, Italy

ARTICLE INFO

Article history:
Received 21 July 2008
Received in revised form 27 November 2008
Accepted 10 February 2009
Available online 21 February 2009

Keywords:
Algebraic turbulence modeling
Annular two-phase flow
Eddy diffusivity
Turbulent viscosity

ABSTRACT

The study considers algebraic turbulence modeling in adiabatic gas–liquid annular two-phase flow. After reviewing the existing literature, two new algebraic turbulence models are proposed for both the liquid film and the droplet laden gas core of annular two-phase flow. Both turbulence models are calibrated with experimental data taken from the open literature and their performance critically assessed. Although the proposed turbulence models reproduce the key parameters of annular flow well (average liquid film thickness and pressure gradient) and the predicted velocity profiles for the core flow compare favorably with available core flow velocity measurements, a more accurate experimental database is required to further improve the models accuracy and range of applicability.

1. Introduction

Annular two-phase flow is one of the most frequently observed flow regimes in gas–liquid two-phase flow systems encountered in the chemical, nuclear and oil industries. Due to its practical interest, annular flow has been the subject of extensive research in the last decades, both experimentally and theoretically. The number of proposed studies dealing with annular flow is actually so huge that no attempt is made here to review the existing literature. Annular flow is characterized by the presence of a thin, wavy liquid film dragged along the channel wall by the shear force exerted by the gas phase, which flows in the center of the channel carrying a part of the liquid phase as entrained droplets. Since the interface between the liquid film and the gas core is highly dynamic and irregularly shaped, gas bubbles occasionally become entrained in the liquid film. The structure and morphology of the interface between the liquid film and the gas core, which is intrinsically time-dependent, strongly affects all transport processes taking place between the phases, thus playing a central role in the overall transport mechanisms and fluid dynamics of annular flow.

Schematically, two types of surface disturbance are typically considered to characterize the interface morphology in annular flow: ripple waves and disturbance waves. Ripple waves are low amplitude and low velocity ripples that appear on top of the liquid film. They are typically short-lived and do not appear to carry liquid mass in the direction of the flow. Disturbance waves, also called roll waves, also appear periodically on the surface of the liquid film and slide on top of the liquid film at a velocity much higher than that of the liquid film surface. The front of disturbance waves rises sharply from the liquid film while their rear tapers off more gradually. The surface of disturbance waves is highly irregular and ruffled, which can result in a characteristic milky appearance as a result of light scattering. Disturbance waves typically form complete rings in the channel, their amplitude can be several times the average liquid film thickness and they tend to live for long axial distances, actively carrying liquid mass in the direction of the flow. If the hydrodynamic conditions are appropriate, the crests of the disturbance waves are sheared-off by the gas flow and liquid droplets become entrained in the gas flow.

Theoretically, annular two-phase flow is particularly difficult to analyze due to the large number of comparable dynamic forces that influence its hydrodynamics. In particular, viscous, inertia and gravity effects are important inside the liquid film, while the drag of the gas flow and surface tension influence the morphology of the liquid–gas interface. Inertia is relevant inside the droplet laden gas core, together with the drag exerted by the gas carrier phase on the entrained liquid droplets which move at a reduced speed in comparison with the gas flow. Droplets are continually entrained from the top of disturbance waves travelling on the liquid film and are eventually redeposited back onto the liquid film. Under steady-state adiabatic flow conditions, the rate of droplet entrainment is balanced by the rate of droplet deposition, so that no net mass transfer takes place between the liquid film and the gas core. Nonetheless, a net exchange of momentum from the gas core to the liquid film is always taking place, since the droplets

* Corresponding author. Tel.: +41 21 693 5981; fax: +41 21 693 5960.
E-mail addresses: andrea.cioncolini@epfl.ch (A. Cioncolini), john.thome@epfl.ch (J.R. Thome), carlo.lombardi@fastwebnet.it (C. Lombardi).
[1] Tel.: +41 21 693 5984; fax: +41 21 693 5960.
[2] Tel.: +39 02 2399 6332, fax: +39 02 2399 6309.

0301-9322/$ - see front matter © 2009 Elsevier Ltd. All rights reserved.
doi:10.1016/j.ijmultiphaseflow.2009.02.002

that are entrained leave the liquid film with a velocity that is typically lower than the velocity of the droplets that are redeposited after being accelerated in the gas core. As such, a tight mass and momentum coupling exists between the phases, further complicating the picture. The above considerations explain why basic modeling of annular two-phase flow is still very limited (Tong and Tang, 1997; Levy, 1999), and presently reliance has to be placed largely on empiricism.

Turbulence is the most common and most complicated form of fluid motion and is one of the last subjects of classical theoretical physics that is still not completely resolved (Bradshaw, 1997; Schmitt, 2007). The correct way to treat turbulent flows is to solve the 3-D time-dependent Navier–Stokes equations, which are currently believed to give an adequate description of turbulent flows (Bradshaw, 1997). This approach, however, is at present too computationally demanding for general engineering applications. Besides, the interest in engineering is typically restricted to a few time-averaged and frequently also space-averaged flow parameters. In order to provide a mean turbulent solution that meets typical engineering needs instead of an instantaneous and local one, the Navier–Stokes equations are typically averaged out in time. The non-linearity of the original system yields a system of averaged equations that contains terms that depend on the small-scale instantaneous turbulent fluctuations. Such terms are collected in the turbulent shear stress tensor which is then related to the average flow quantities, thus providing a turbulence model to properly close the time-averaged system.

Several turbulence models have been proposed so far (Wilcox, 2002), with algebraic models being the simplest of all. Algebraic models utilize the Boussinesq assumption that considers the turbulent shear stress to be proportional to the symmetric part of the gradient of the mean velocity field. The constant of proportionality, which is referred to as the turbulent viscosity or eddy viscosity, depends upon the flow and is expressed by an empirical algebraic relation that involves the length scales of the mean flow. Notwithstanding the limitations of the Boussinesq assumption (Schmitt, 2007) and its highly simplified character, algebraic models are easy to use, easy to implement and typically are reasonably accurate for many engineering applications (Tannehill et al., 1997; Wilcox, 2002). Being empirical, these models typically work well only within the limits of the original experimental database they have been fine-tuned with.

Numerous studies have addressed turbulence in annular two-phase flow (Anderson and Mantzouranis, 1960; Hewitt and Lacey, 1965; Levy, 1966; Moeck and Stachiewicz, 1972; Butterworth, 1974; Ueda and Nose, 1974; Ueda and Tanaka, 1974; Levy and Healzer, 1981; Dobran, 1983; Tandon et al., 1985; Abolfald and Wallis, 1986; Oliemans et al., 1986; Jensen, 1987; Bellinghausen and Renz, 1992; Malamatenios et al., 1994; Jayanti and Hewitt, 1997; Azzopardi, 1999; Kaji et al., 1999; Trabold and Kumar, 1999; Vassallo, 1999; Kumar and Trabold, 2000; Kishore and Jayanti, 2004; Pu et al., 2006; Peng, 2008), both experimentally and theoretically. Most of the time, turbulence modeling has been dealt with indirectly, as an intermediate step in the context of general annular flow modeling for experimental data reduction and/or the prediction of hydraulic parameters.

Turbulence in the liquid film has attracted particular interest, due to its connection with the theoretical prediction of the heat transfer coefficient and the onset of dryout in boiling channels. Due to the highly dynamic morphology of the liquid film, the experimental investigation of turbulence is particularly challenging. Vassallo (1999) experimentally investigated the turbulence structure in the wall region of air–water annular flow. For thin liquid films, Vassallo (1999) found that the turbulence structure was similar to that of single-phase wall-bounded flows. For thick liquid films, however, the turbulence structure was found to be modified by the highly dynamic character of the gas–liquid interface. Numerical simulations performed by Jayanti and Hewitt (1997) suggest that disturbance waves may behave as packages of turbulence sliding on top of a laminar substrate liquid film. Turbulence in the liquid film, therefore, seems to be strongly linked to the liquid film morphology in general and to the disturbance wave dynamics in particular.

In the majority of the available studies, turbulence modeling in the annular liquid film has been carried out by extrapolating the results of algebraic turbulence modeling in single-phase wall-bounded flow (Anderson and Mantzouranis, 1960; Hewitt and Lacey, 1965; Levy, 1966; Butterworth, 1974; Ueda and Nose, 1974; Ueda and Tanaka, 1974; Tandon et al., 1985; Abolfald and Wallis, 1986; Oliemans et al., 1986; Kishore and Jayanti, 2004; Pu et al., 2006; Peng, 2008), with some researchers (Kaji et al., 1999; Vassallo, 1999) proposing slight modifications to the single-phase flow theory to better capture the unique features of annular flow. On the basis of direct observations of annular flow, some researchers (Moeck and Stachiewicz, 1972; Ueda and Nose, 1974; Ueda and Tanaka, 1974) proposed that the liquid film might be decomposed into two sub layers: a continuous liquid base layer in contact with the channel wall below an intermittent and wavy liquid layer extending to the liquid-gas interface. Accordingly, two-layer turbulence models for the liquid film have been proposed (Moeck and Stachiewicz, 1972; Levy and Healzer, 1981; Dobran, 1983), providing a potentially superior description of the liquid film turbulence structure. The two-layer algebraic model proposed by Dobran (1983), in particular, is probably the most successful (Jensen, 1987; Malamatenios et al., 1994). The increased accuracy of two-layer models comes about at the expense of an increased number of empirical correlations required to actually implement these models. In the model of Dobran (1983), besides the correlations for predicting the turbulent viscosity in both the continuous base liquid layer and in the intermittent liquid layer, a further correlation is provided to estimate the thickness of the continuous base liquid layer. Typical values for this key parameter are in the range of 10^{-5}–10^{-4} m, small enough to make experimental measurements to verify the existence of two sub layers particularly challenging and their outcome potentially questionable, due to several second-order effects that might influence the measurements and should therefore be taken into account, such as the radial swelling of the tube under pressure load or misalignments and meniscus occurrence if the needle contact measuring technique is used. Since algebraic turbulence modeling is empirical in nature, the possibility to easily collect experimental data to fine-tune the models is of crucial importance. In this respect, the smaller the number of empirical correlations required to feed an algebraic turbulence model, the better. Besides, having to rely on challenging and potentially questionable experiments to collect the required data is a significant drawback that severely limits the usefulness of an algebraic turbulence model and should be avoided, even perhaps at the expense of lower accuracy in the model predictions.

The available experimental studies that address turbulence in the gas core of annular two-phase flow (Azzopardi, 1999; Trabold and Kumar, 1999) seem to indicate a higher turbulent intensity in annular flow with respect to a comparable single-phase gas flow. This enhancement of turbulence can be traced to the interaction of the gas flow with both the liquid film and the entrained liquid droplets. In particular, the highly irregular liquid film that surrounds the gas core is believed to act as a sort of surface roughness that affects the gas flow, increasing the turbulence intensity. The entrained droplets move slower than the carrier gas, are present in a broad distribution of sizes, can be highly deformed and are believed to actively shed vortices, thus increasing the turbulence intensity in the gas core. In analogy with what was already discussed for the liquid film, turbulence modeling in the gas core

has mostly been carried out by extrapolating the results of algebraic turbulence modeling in single-phase wall-bounded flow (Abolfald and Wallis, 1986; Bellinghausen and Renz, 1992; Kaji et al., 1999; Peng, 2008), with all researchers proposing modifications to the single-phase flow theory to better capture the unique features of annular flow.

What emerges from the existing literature regarding algebraic turbulence modeling in annular two-phase flow is that the results valid for single-phase wall-bounded flow can to a good extent be extrapolated to both the liquid film and the gas core. For the liquid film, in particular, the direct application of single-phase flow theory seems to be generally acceptable, at least as a first order approximation of thin films. Thick films, however, may require some improvement to better capture the peculiarities of annular flow, especially if the boiling heat transfer coefficient prediction is of concern, since the direct application of single-phase flow theory is likely to overpredict the turbulence intensity and the heat transfer rate through the liquid film (Hewitt, 1998). Two-layer models, though potentially more accurate, are hampered by the procurement of the precise experimental data required for their calibration. For what concerns the gas core, on the other hand, the direct application of single-phase flow theory is still the starting point but some tailoring of the theory on annular flow seems necessary to get acceptable predictions. It is worth noting that besides algebraic turbulence models, also the more sophisticated κ–ε turbulence model (Wilcox, 2002) for single-phase flow has been applied to annular flow (Bellinghausen and Renz, 1992; Jayanti and Hewitt, 1997; Kumar and Trabold, 2000) with some success.

The purpose of the present study is to propose new algebraic turbulence models for both the liquid film and the droplet laden gas core for adiabatic, fully developed annular two-phase flow, calibrated with a data bank collected from the open literature (Hall-Taylor et al., 1963; Silvestri et al., 1963; Adorni et al., 1963; Casagrande et al., 1963; Cravarolo et al., 1964; Gill et al., 1964, 1965; Shearer and Nedderman, 1965; Saito et al., 1978). Special care is taken in keeping the number of empirical tuning parameters to a minimum and to limit the experimental information required to fine-tune the models to a few, easily accessible macroscopic flow parameters. As will be shown, the experimental information required to calibrate the proposed models is essentially limited to the total mass flow rates of the two phases, the total pressure gradient and the average liquid film thickness. The present study is limited to turbulent momentum transport. Since internal energy and other passive contaminants are transported by turbulence roughly in the same way as momentum (Bradshaw, 1997), the information provided in the present study can be used as a starting point for more advanced modeling of annular flow, such as the rate of convective boiling and condensation heat transfer in diabatic flows.

2. Model description

Newton's law of friction, together with the Boussinesq assumption for turbulence modeling, yields the first-order, ordinary differential equations that the velocity profile must satisfy in both the liquid film and the gas core, respectively:

$$(\mu_l + \mu_{t-lf})\frac{dV_{lf}}{dy} = \tau_{lf}(y), \quad 0 \le y \le t \tag{1}$$

$$(\mu_c + \mu_{t-gc})\frac{dV_{gc}}{dy} = \tau_{gc}(y), \quad t \le y \le R \tag{2}$$

where μ_l and μ_c are the liquid and droplet-laden gas core viscosities, respectively, V_{lf} and V_{gc} are the velocities in the liquid film and in the gas core and τ_{lf} and τ_{gc} are the shear stresses in the liquid film and in the gas core while y, t and R are the distance from the channel wall, the average liquid film thickness and the tube radius, respectively. As can be seen, Eqs. (1) and (2) are formally analogous to the corresponding equations that hold for laminar flow. Turbulence is taken care of by the introduction of the turbulent viscosities $\mu_{t\text{-}lf}$ and $\mu_{t\text{-}gc}$, which are flow dependent and cause the viscosity to seem much greater than it actually is. Then, in order to express the shear stresses in the liquid film τ_{lf} and in the gas core τ_{gc}, a model for annular flow is required. In the present study, annular flow modeling is carried out in the framework of the following simplifying assumptions:

1. Fully-developed, steady-state adiabatic, co-current annular flow.
2. The entrainment and deposition processes are at equilibrium, and no net mass transfer takes place between the liquid film and the gas core.
3. The slip between the carrier gas flow and the entrained liquid droplets is neglected, i.e. the gas and entrained droplets are assumed to travel at the same velocity.
4. All thermo-physical properties are assumed to be constant with the exception of the density of the gas phase, which depends on the local pressure.
5. Cylindrical symmetry of the flow is assumed, and any circumferential variation of the liquid film thickness is neglected.
6. The total mass flow rates of both the liquid and gas phases, together with the average liquid film thickness and the total pressure drop, are assumed to be known experimentally to close the model. The pressure gradient is estimated as follows:

$$\frac{dP}{dz} \approx -\frac{|\Delta P_{tot}|}{L_{dp}} \tag{3}$$

where ΔP_{tot} is the total pressure drop, L_{dp} is the distance between the pressure taps and z is the axial coordinate along the channel. Assumption 2 can be considered to be acceptable for adiabatic two-phase, two-component flow where evaporation and flashing are not taking place and far enough from the location in the flow system where the two phases are actually mixed together. Existing evidence (Fore and Dukler, 1995; Azzopardi, 1997, 1999) reveals that the slip between the carrier gas and the entrained droplets is typically small, so that assumption 3 is believed to be acceptable. It is worth highlighting that relaxation of this assumption would require the size distribution, the shape distribution and the velocity distribution of the entrained droplets to be specified or predicted and such detailed information is at present largely unavailable. The same remark holds for the drag of the gas flow on the entrained droplets. In adiabatic systems only the pressure variation can affect the thermo-physical properties of the fluids, which with the exception of the gas phase are quite insensitive to pressure. As such, assumption 4 is considered acceptable. Allowing the gas density to vary with pressure allows the model to capture the acceleration of the gas phase along the channel, as a consequence of the specific volume increase triggered by the pressure reduction experienced as the fluid flows along the channel. Assumption 5 is generally acceptable for vertical flow, while for horizontal and inclined flow it is acceptable provided that the mass flux is high enough to prevent gravity from breaking the symmetry of the flow. The experimental data used in the present study refer to vertical upflow. Assumption 6 may appear to be rather arbitrary and deserves some special comment. Algebraic turbulence modeling is empirical in nature, so that at some point theoretical considerations have to be merged with experimental data to properly close the problem. Assumption 6 is actually inspired by the structure of the experimental database used in the present analysis, which includes data for the total mass flow rates of the phases, the average liquid film thickness and the total pressure drop along the test section. Concerning the pressure gradi-

ent, in particular, Eq. (3) is exact in the limit of a linear pressure profile along the channel. Due to the acceleration of the gas phase, however, the pressure profile is never strictly linear. Nonetheless, within the limits of the present study the approximation implied by the use of Eq. (3) is considered acceptable.

The conservation of linear momentum, together with these six assumptions, allows the shear stresses for both the liquid film and the gas core to be calculated as follows:

$$\tau_{lf}(y) = \frac{1}{1-\xi}\left(1-\frac{y}{R}-\frac{\xi R}{R-y}\right)\tau_w + \frac{y(2R-y)}{2(R-y)}\left(\rho_l - \frac{\rho_{mix}}{1-\xi}\right)g\sin\theta \approx \frac{1}{1-\xi}\left(1-\frac{y}{R}-\frac{\xi R}{R-y}\right)\tau_w + y\left(\rho_l - \frac{\rho_{mix}}{1-\xi}\right)g\sin\theta, \quad 0 \le y \le t \tag{4}$$

$$\tau_{gc}(y) = \frac{1}{1-\xi}\left(1-\frac{y}{R}\right)\tau_w + \frac{1}{2}(R-y)\left(\frac{\rho_{mix}}{1-\xi} - \rho_c\right)g\sin\theta, \quad t \le y \le R \tag{5}$$

where τ_w is the wall shear stress, ρ_l and ρ_c are the liquid and droplet-laden gas core densities, respectively, ρ_{mix} is the cross sectional average density, g is the acceleration of gravity and θ is the channel inclination angle with respect to the horizontal ($\theta = 0$ for horizontal flow). A detailed derivation of Eqs. (4) and (5) is included in Appendix A. The experimental data bank used in the present study covers both thin and thick liquid films, so that curvature effects cannot be neglected. The second term appearing on the right-hand side of Eq. (4) is a gravitational correction that is typically an order of magnitude smaller than the first term. As such, it is acceptable to neglect curvature effects for this corrective term only and simplify the expression for the shear stress in the liquid film as indicated.

The dimensionless parameter ξ appearing in Eqs. (4) and (5) accounts for the acceleration of the gas phase along the channel and is calculated as follows:

$$\xi = \frac{x^2 G^2}{\varepsilon}\left|\frac{dv_g}{dP}\right| \tag{6}$$

where x is the vapor quality, G is the total mass flux, v_g is the gas specific volume and P is the pressure. The sensitivity of the gas specific volume to the variation of the operating pressure is estimated from REFPROP (2007), as all other properties of the fluids. As schematically indicated in Fig. 1, the parameter ε is the void fraction, which represent the fraction of the channel cross sectional area occupied by the gas phase, while the parameter γ is the liquid droplet hold-up, representing the fraction of the liquid phase cross sectional area occupied by the entrained droplets. The two parameters ε and γ are related as follows:

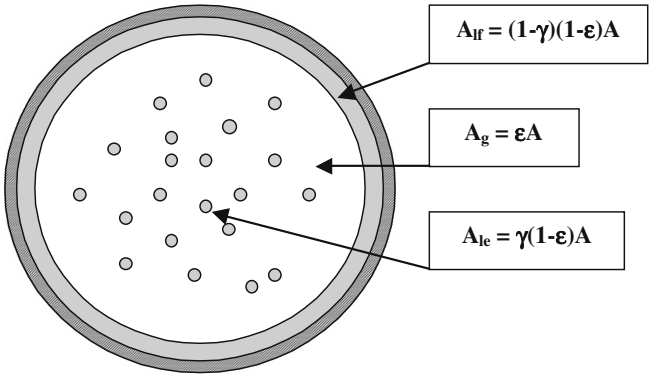

Fig. 1. Schematic representation of the cross sectional area A split among the phases.

$$(1-\varepsilon)(1-\gamma) = \frac{t(2R-t)}{R^2} \tag{7}$$

$$\gamma\frac{1-\varepsilon}{\varepsilon} = e\frac{1-x}{x}\frac{\rho_g}{\rho_l} \tag{8}$$

where ρ_g is the density of the gas and e is the fraction of liquid entrained in the gas core. Eq. (7) corresponds to the analytical expression of the liquid film flow area, while Eq. (8) implements assumption 3 of no slip between the carrier gas and the entrained droplets. Eqs. (7) and (8) constitute a system of two equations that can be solved for the unknowns ε and γ provided that the right-hand sides of both equations are known. In this respect, the only parameter that needs to be determined is the fraction of liquid entrained e, which is estimated from a correlation proposed by Oliemans et al. (1986):

$$\frac{e}{1-e} = 10^{b_0}\rho_l^{b_1}\rho_g^{b_2}\mu_l^{b_3}\mu_g^{b_4}\sigma^{b_5}d^{b_6}J_l^{b_7}J_g^{b_8}g^{b_9} \tag{9}$$

where μ_g is the gas viscosity, σ is the surface tension, d is the tube diameter and J_l and J_g are the superficial liquid and gas velocities:

$$J_l = \frac{(1-x)G}{\rho_l} \tag{10}$$

$$J_g = \frac{xG}{\rho_g} \tag{11}$$

The exponents b_0–b_9 appearing in Eq. (9) are summarized in Table 1 as function of the liquid film Reynolds number, which is defined as follows:

$$Re_{lf} = \frac{4}{\pi}\frac{(1-e)\Gamma_l}{\mu_l d} \tag{12}$$

where Γ_l is the liquid mass flow rate. A constraint to the values of the exponents b_0–b_9 in Eq. (9) is that the right-hand side of Eq. (9) forms a dimensionless group. As can be seen in Eq. (12), the liquid film Reynolds number depends on the fraction of liquid entrained e, so that an iterative calculation is required. Operatively, a first order estimate for e is obtained using the values b_0–b_9 from Table 1 which are applicable irrespective of the liquid film Reynolds number. The Reynolds number of the liquid film can then be calculated, and the estimate for e accordingly refined. The procedure is then repeated, with 2–3 steps typically required to converge. The correlation of Oliemans et al. (1986) is based on a database compiled at AERE Harwell which contains about 700 experimental points obtained with air–water, air–ethanol, air–genklene and steam–water covering tube diameters from 6.0 mm to 31.8 mm and operating pressures from nearly atmospheric to 9.0 MPa and appears particularly appropriate for use in the present study since a part of the experimental data used to develop Eq. (9) is actually included in the data bank used here to calibrate the turbulence models. The wall shear stress τ_w appearing in Eqs. (4) and (5) is calculated from the conservation of linear momentum for the total flow as follows:

$$\tau_w = \frac{R}{2}\left[(1-\xi)\frac{|\Delta P_{tot}|}{L_{dp}} - \rho_{mix}g\right] \tag{13}$$

According with assumption 3, the droplet laden core flow density ρ_c is calculated on a homogeneous flow basis for the core flow as follows (Levy, 1999):

$$\rho_c = (1-\varepsilon_c)\rho_l + \varepsilon_c\rho_g \tag{14}$$

where ε_c is the void fraction of the core flow:

$$\varepsilon_c = \frac{\varepsilon}{\varepsilon + \gamma(1-\varepsilon)} \tag{15}$$

The total mixture density ρ_{mix} is calculated on a void fraction mixing basis as follows:

$$\rho_{mix} = (1-\varepsilon)\rho_l + \varepsilon\rho_g \tag{16}$$

The two differential equations for the velocity profiles in the liquid film and in the gas core are obtained upon substitution of Eqs. (4) and (5) into Eqs. (1) and (2), respectively. The dimensionless form of the differential expression for the liquid film reads as follows:

$$\in_{lf}^{+}\frac{dV_{lf}^{+}}{dy^{+}} = \frac{1}{1-\xi}\left(1-\frac{y^{+}}{R^{+}}-\frac{\xi R^{+}}{R^{+}-y^{+}}\right)+C_{lf}y^{+}, \quad 0\le y^{+}\le t^{+} \tag{17}$$

$$V_{lf}^{+}(0) = 0 \tag{18}$$

$$C_{lf} = \frac{(y^{*})^{2}}{\mu_l V^{*}}\left(\rho_l - \frac{\rho_{mix}}{1-\xi}\right)g\sin\theta \tag{19}$$

The liquid film dimensionless variables appearing in Eq. (17) are defined as follows:

$$\in_{lf}^{+} = 1+\frac{\mu_{t-lf}}{\mu_l}; \quad V_{lf}^{+} = \frac{V_{lf}}{V^{*}}; \quad y^{+} = \frac{y}{y^{*}}; \quad R^{+} = \frac{R}{y^{*}}; \quad t^{+} = \frac{t}{y^{*}} \tag{20}$$

The liquid film velocity and length scales are defined as follows:

$$V^{*} = \sqrt{\frac{\tau_w}{\rho_l}}; \quad y^{*} = \frac{\mu_l}{\rho_l V^{*}} \tag{21}$$

The dimensionless form of the differential expression for the gas core reads as follows:

$$\in_{gc}^{\sim}\frac{dV_{gc}^{\sim}}{dy^{\sim}} = \frac{1}{1-\xi}\left(1-\frac{y^{\sim}}{R^{\sim}}\right)+C_{gc}(R^{\sim}-y^{\sim}), \quad t^{\sim}\le y^{\sim}\le R^{\sim} \tag{22}$$

$$V_{gc}^{\sim}(t^{\sim}) = \sqrt{\frac{\rho_c}{\rho_l}}V_{lf}^{+}(t^{+}) \tag{23}$$

$$C_{gc} = \frac{(y^{\S})^{2}}{2\mu_c V^{\S}}\left(\frac{\rho_{mix}}{1-\xi}-\rho_c\right)g\sin\theta \tag{24}$$

The gas core dimensionless variables appearing in Eq. (22) are defined as follows:

$$\in_{gc}^{\sim} = 1+\frac{\mu_{t-gc}}{\mu_c}; \quad V_{gc}^{\sim} = \frac{V_{gc}}{V^{\S}}; \quad y^{\sim} = \frac{y}{y^{\S}}; \quad R^{\sim} = \frac{R}{y^{\S}}; \quad t^{\sim} = \frac{t}{y^{\S}} \tag{25}$$

The gas core velocity and length scales are defined as follows:

$$V^{\S} = \sqrt{\frac{\tau_w}{\rho_c}}; \quad y^{\S} = \frac{\mu_c}{\rho_c V^{\S}} \tag{26}$$

According with assumption 3, the droplet laden core flow viscosity μ_c is calculated on a homogeneous flow basis for the core flow as follows (Levy, 1999):

$$\mu_c = (1-\varepsilon_c)\mu_l + \varepsilon_c\mu_g \tag{27}$$

A no-slip boundary condition has been applied at the wall for the liquid film velocity profile, Eq. (18), while continuity of the velocity profile across the liquid-gas interface is used as a boundary condition for the gas core velocity profile, Eq. (23). This, of course, yields a tight coupling between the two velocity profiles. In order to carry out the integration and obtain the velocity profiles, two algebraic turbulence models are required to express the eddy diffusivities $\in_{lf}^{+}$ and $\in_{gc}^{\sim}$ as functions of the length scales characteristic of the problem, where the length scale can be thought of as a measure of the turbulent eddy size typical of the flow of interest. The turbulent structure in the liquid film, in particular, is assumed to be mostly affected by the interaction of the liquid film with the gas flow, as though the liquid film behaved as a fluid-bounded flow, such as a mixing layer or a jet, with a negligible influence of the bounding wall. This assumption is actually suggested by the structure of the liquid film flow already discussed in the Introduction, characterized by the disturbance waves that behave as packages of turbulence that slide under the gas shear on top of a very thin liquid substrate. Accordingly, the characteristic length scale for the liquid film is assumed to be the average liquid film thickness, and the liquid film eddy diffusivity is schematically expressed as follows:

$$\in_{lf}^{+} = f(t^{+}) \tag{28}$$

Being independent of the variable of integration y^{+} in Eq. (17), the eddy diffusivity $\in_{lf}^{+}$ can be taken out of the integral without having to specify at this point the functional relationship schematically indicated in Eq. (28) that will be determined through comparison with experimental data, as it will be shown in the following section.

The turbulent structure in the gas core, on the other hand, is assumed to be mostly affected by the presence of the wall, as typically happens with wall-bounded flows in general and pipe flow in particular. The presence of the sliding liquid film is felt through the boundary condition of the problem, Eq. (23). Accordingly, the characteristic length scale for the gas flow is assumed to be the distance from the wall, and the gas core eddy diffusivity is schematically expressed as follows:

$$\in_{gc}^{\sim} = f(y^{\sim}) \tag{29}$$

Since the eddy diffusivity $\in_{gc}^{\sim}$ depends on the variable of integration $y^{\sim}$ in Eq. (22), it is necessary to further specify the symbolic relationship in Eq. (29). In principle, any algebraic relation involving the length scale $y^{\sim}$ might be tested, and its applicability checked through comparison with experimental data. In the present study different relations were tested and a simple linear dependence involving one empirical parameter a, as indicated in Eq. (30), was found to provide an acceptable fit of the available experimental data, as will be shown in the following section.

$$\in_{gc}^{\sim} = \frac{1}{a}y^{\sim} \tag{30}$$

More sophisticated relations for the core flow eddy diffusivity were not found to yield any appreciable gain in accuracy. The experimental database used in the present study is limited, so that it is worth highlighting that the algebraic turbulence model proposed in Eq. (30) should be considered as a first approximation, which may require refinement should a more extended and accurate experimental database become available. By using the turbulence models expressed by Eqs. (28) and (30) it is possible to carry out the integrations in Eqs. (17) and (22) and thus obtain the velocity profiles for the liquid film and the gas core:

Table 1
Parameters for Oliemans et al. correlation, Eq. (9).

Re_{lf}	b_0	b_1	b_2	b_3	b_4	b_5	b_6	b_7	b_8	b_9
All values	−2.52	1.08	0.18	0.27	0.28	−1.80	1.72	0.70	1.44	0.46
10^2–3×10^2	−0.69	0.63	0.96	−0.80	0.09	−0.88	2.45	0.91	−0.16	0.86
3×10^2–10^3	−1.73	0.94	0.62	−0.63	0.50	−1.42	2.04	1.05	0.96	0.48
10^3–3×10^3	−3.31	1.15	0.40	−1.02	0.46	−1.00	1.97	0.95	0.78	0.41
3×10^3–10^4	−8.27	0.77	0.71	−0.13	−1.18	−0.17	1.16	0.83	1.45	−0.32
10^4–3×10^4	−6.38	0.89	0.70	−0.17	−0.55	−0.87	1.67	1.04	1.27	0.07
3×10^4–10^5	−0.12	0.45	0.25	0.86	−0.05	−1.51	0.91	1.08	0.71	0.21

$$V_{lf}^{+}=\frac{1}{\in_{lf}^{+}}\left\{\frac{1}{1-\xi}\left[y^{+}-\frac{(y^{+})^{2}}{2R^{+}}+\xi R^{+}\ln\left(1-\frac{y^{+}}{R^{+}}\right)\right]+\frac{1}{2}C_{lf}(y^{+})^{2}\right\},\quad 0\le y^{+}\le t^{+} \tag{31}$$

$$V_{gc}^{\sim}=\sqrt{\frac{\rho_c}{\rho_l}}V_{lf}^{+}(t^{+})+a\left(\frac{1}{1-\xi}+C_{gc}R^{\sim}\right)\left[\ln\left(\frac{y^{\sim}}{t^{\sim}}\right)-\frac{y^{\sim}-t^{\sim}}{R^{\sim}}\right],\quad t^{\sim}\le y^{\sim}\le R^{\sim} \tag{32}$$

The velocity profile in the liquid film depends on the eddy diffusivity $\in_{lf}^{+}$, which is an arbitrary function of the average liquid film thickness t^{+}, while the velocity profile in the gas core depends on the arbitrary constant a. A block-diagram illustrating the actual implementation of the annular flow model described so far is included in Appendix B.

3. Model calibration

The algebraic turbulence models assumed in Eqs. (28) and (30) are calibrated as follows. The mass flow rates of the liquid film Γ_{lf} and the gas core Γ_{gc} can be calculated by integrating the respective velocity profiles, Eqs. (31) and (32) as follows:

$$\Gamma_{lf}=(1-e)\Gamma_l=2\pi\rho_l\int_0^t V_{lf}(y)(R-y)dy \tag{33}$$

$$\Gamma_{gc}=e\Gamma_l+\Gamma_g=2\pi\rho_c\int_t^R V_{gc}(y)(R-y)dy \tag{34}$$

where Γ_g is the gas mass flow rate. After rearranging, the eddy diffusivity $\in_{lf}^{+}$ in the liquid film and the constant a for the core flow can be expressed as:

$$\in_{lf}^{+}=\frac{\pi\rho_l V^{*}(y^{*})^{2}}{(1-e)\Gamma_l}\left(\frac{1}{1-\xi}\left\{R^{+}(t^{+})^{2}\left(1-\frac{t^{+}}{2R^{+}}\right)^{2}+\xi(R^{+})^{3}\left[\left(1-\frac{t^{+}}{R^{+}}\right)^{2}\left(\frac{1}{2}-\ln\left(1-\frac{t^{+}}{R^{+}}\right)\right)-\frac{1}{2}\right]\right\}+C_{lf}(t^{+})^{3}\left(\frac{R^{+}}{3}-\frac{t^{+}}{4}\right)\right) \tag{35}$$

$$a=\frac{\frac{e\Gamma_l+\Gamma_g}{2\pi\rho_c V^{\S}(y^{\S})^{2}}-\frac{1}{2}\sqrt{\frac{\rho_c}{\rho_l}}V_{lf}^{+}(t^{+})(R^{\sim}-t^{\sim})^{2}}{\left(\frac{1}{1-\xi}+C_{gc}R^{\sim}\right)\left[\frac{1}{2}(R^{\sim})^{2}\ln\left(\frac{R^{\sim}}{t^{\sim}}\right)-\frac{3}{4}(R^{\sim})^{2}+R^{\sim}t^{\sim}-\frac{(t^{\sim})^{2}}{4}-\frac{(R^{\sim}-t^{\sim})^{3}}{6R^{\sim}}\right]} \tag{36}$$

Both the eddy diffusivity $\in_{lf}^{+}$ in the liquid film and the constant a for the core flow can be calculated from Eqs. (35) and (36) if experimental data are available. In particular, it can be seen that the experimental information required to carry out the calculations is limited to (i) the mass flow rate of each phase, (ii) the average liquid film thickness and (iii) the total pressure drop, together with the annular flow model discussed in Section 2. This small number of easily accessible flow parameters required for the calibration of the turbulence models is a significant advantage with respect to more sophisticated approaches, such as two-layer models. As already pointed out, algebraic turbulent models work well only for the flows they have been fine-tuned for. In this respect, the possibility to easily extend the experimental database used for calibration is of crucial importance.

The main details of the experimental data bank used in the present study, which has been collected from the open literature, are summarized in Table 2 (Hall-Taylor et al., 1963; Silvestri et al., 1963; Adorni et al., 1963; Casagrande et al., 1963; Cravarolo et al., 1964; Gill et al., 1964, 1965; Shearer and Nedderman, 1965; Saito et al., 1978). CISE researchers (Silvestri et al., 1963; Adorni et al., 1963; Casagrande et al., 1963; Cravarolo et al., 1964) studied water-argon and water-nitrogen adiabatic annular flow at operating conditions selected to mimic boiling water for nuclear reactor applications. The operating conditions were varied during the tests in order to modify both the density and the viscosity of the fluids, while alcohol was added to the water in some of the tests with argon in order to modify the surface tension as well. All other investigations (Hall-Taylor et al., 1963; Gill et al., 1964, 1965; Shearer and Nedderman, 1965; Saito et al., 1978) were carried out with water and air as the test fluids at operating pressures close to atmospheric pressure. It is worth noting that only a selection of the Whalley original data (Whalley et al., 1974) compiled by Saito et al. (1978) is used in the present study, as the Whalley original report was not available. All the tests refer to vertical, adiabatic annular upflow through circular pipes. The measured flow parameters are the mass flow rate of each phase, the total pressure drop and the average liquid film thickness, the latter parameter being measured by all investigators with the electrical conductivity technique. The experimental uncertainties of the key parameters in the present study are summarized in Table 3.

Besides the use of different fluids and different operating conditions, the chief difference among the investigations that comprise the data bank is the use of different mixing devices to actually mix the two phases together before the test section. Existing evidence (Wolf et al., 2001) shows that adiabatic annular flow may be quite slow in reaching fully developed flow conditions and loose any memory effect of the mixing device. The equilibrium entrained liquid fraction and the average liquid film thickness, in particular, appear to be the slowest hydrodynamic parameters to respond and

Table 3
Experimental uncertainties.

Mass flow rate	2.0%
Average liquid film thickness	3.5%
Total pressure drop	1–15%
Tube inner diameter	1.0%
Tube length	1.0%
Equilibrium liquid entrained fraction*	10.0%

* Assumed.

Table 2
Experimental data bank.

Reference	Fluids	d (mm)	P (MPa)	G (kg m^{-2} s^{-1})	x	Mixer type	L/d^{*}	No. points
CISE (Silvestri et al., 1963; Adorni et al., 1963; Casagrande et al., 1963; Cravarolo et al., 1964)	H_2O–argon H_2O–alcohol–argon H_2O–nitrogen	15.1 25.0	0.6–2.1	300–3000	0.05–0.85	(1)	53–220	1201
Gill (Gill et al., 1964; Gill et al., 1965; Shearer and Nedderman, 1965)	H_2O–air	31.7	0.1–0.2	20–600	0.10–0.95	(1) – (2) – (3)	~70	138
Whalley (Saito et al., 1978)	H_2O–air	31.7	0.3–0.4	150–300	0.20–0.85	n.a.	n.a.	15
Hall-Taylor (Hall-Taylor et al., 1963)	H_2O–air	31.7	0.1–0.2	20–80	0.40–0.80	(2)	~180	18

(1) Annular slot.
(2) Porous sinter.
(3) Multi-Jet.
* Distance from mixer.

can show some residual dependence on inlet conditions even after 100–300 tube diameters. The entrained droplets concentration might be even slower in reaching steady-state flow conditions, according to existing evidence regarding solid particle-laden gas flows (Marchioli et al., 2008). In principle, therefore, all the experimental data collected in the data bank might be affected by a residual dependence on inlet conditions. If all the experimental data were collected using the same mixing device some bias might be expected in the data bank. The use of different mixing devices, on the other hand, should prevent the biasing of the data, probably at the expense of some extra scattering.

All the pertinent details regarding the experimental facilities, the measuring techniques and their validations can be found in the original reports. In order to further validate the experimental data, together with the proposed model for annular flow, the results regarding the void fraction calculated from Eqs. (7) and (8) are compared in Figs. 2–4 with the predictions of the homogeneous model and with the predictions of the empirical correlations due to Lockhart and Martinelli (1949) and Woldesemayat and Ghajar (2007). In the framework of the homogeneous model for one-dimensional two-phase flow, the slip between the phases is neglected and the void fraction can correspondingly be calculated as follows:

$$\varepsilon = \left[1 + \frac{\rho_g}{\rho_l}\left(\frac{1-x}{x}\right)\right]^{-1} \tag{37}$$

As noted by Butterworth (1975) the empirical correlation of Lockhart and Martinelli (1949) is well represented by the relation:

$$\varepsilon = \left(1 + 0.28\chi_{tt}^{0.71}\right)^{-1} \tag{38}$$

where χ_{tt} is the turbulent-turbulent Martinelli parameter:

$$\chi_{tt} = \left(\frac{1-x}{x}\right)^{0.9}\left(\frac{\rho_g}{\rho_l}\right)^{0.25}\left(\frac{\mu_l}{\mu_g}\right)^{0.1} \tag{39}$$

The empirical correlation of Woldesemayat and Ghajar (2007) reads as follows:

$$\varepsilon = \frac{J_g}{J_g\left[1 + \left(\frac{J_l}{J_g}\right)^{\left(\frac{\rho_g}{\rho_l}\right)^{0.1}}\right] + 2.9\left[\frac{gd\sigma(1+\cos\theta)(\rho_l-\rho_g)}{\rho_l^2}\right]^{0.25}(1.22+1.22\sin\theta)^{\frac{P_{atm}}{P}}} \tag{40}$$

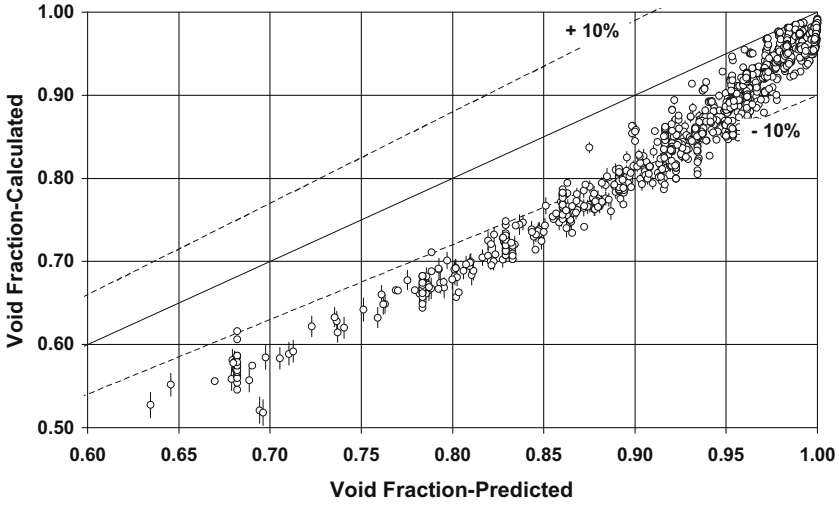

Fig. 2. Comparison of calculated void fraction values with the homogeneous model predictions, Eq. (37).

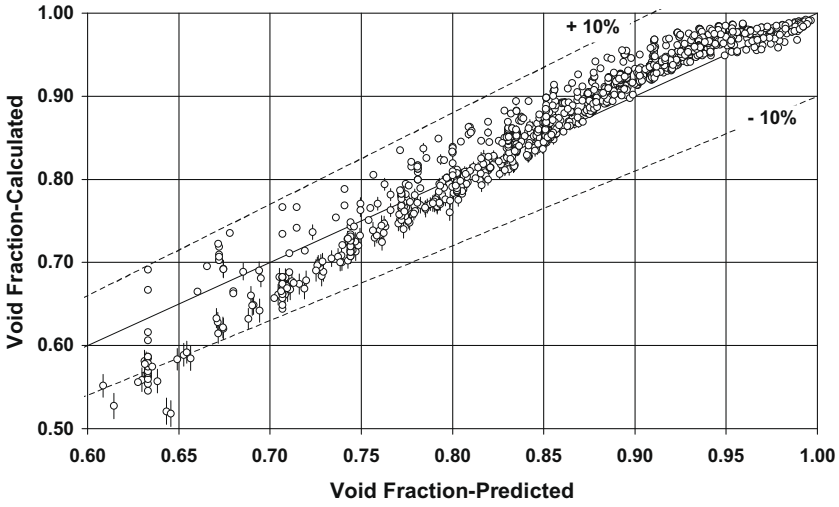

Fig. 3. Comparison of calculated void fraction values with the Lockhart and Martinelli correlation predictions, Eq. (38).

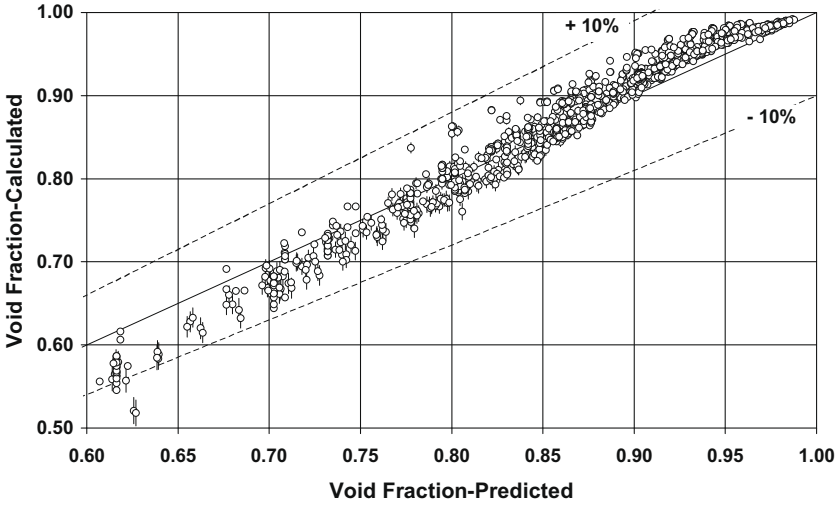

Fig. 4. Comparison of calculated void fraction values with the Woldesemayat and Ghajar correlation predictions, Eq. (40).

where the numerical constant 2.9 appearing in Eq. (40) has the dimension $m^{-0.25}$, θ is the channel inclination angle with respect to the horizontal ($\theta = 0$ for horizontal flow), P_{atm} is atmospheric pressure and P is the system pressure. The homogeneous model handles effectively all two-phase flows characterized by a fine mixing of the phases, such as bubbly flow and mist flow, while it should be avoided whenever there is a tendency of the phases to become segregated and consequently develop a slip. Its use in the context of annular flow, therefore, is really inappropriate. Nonetheless, in the framework of one-dimensional co-current two-phase flow

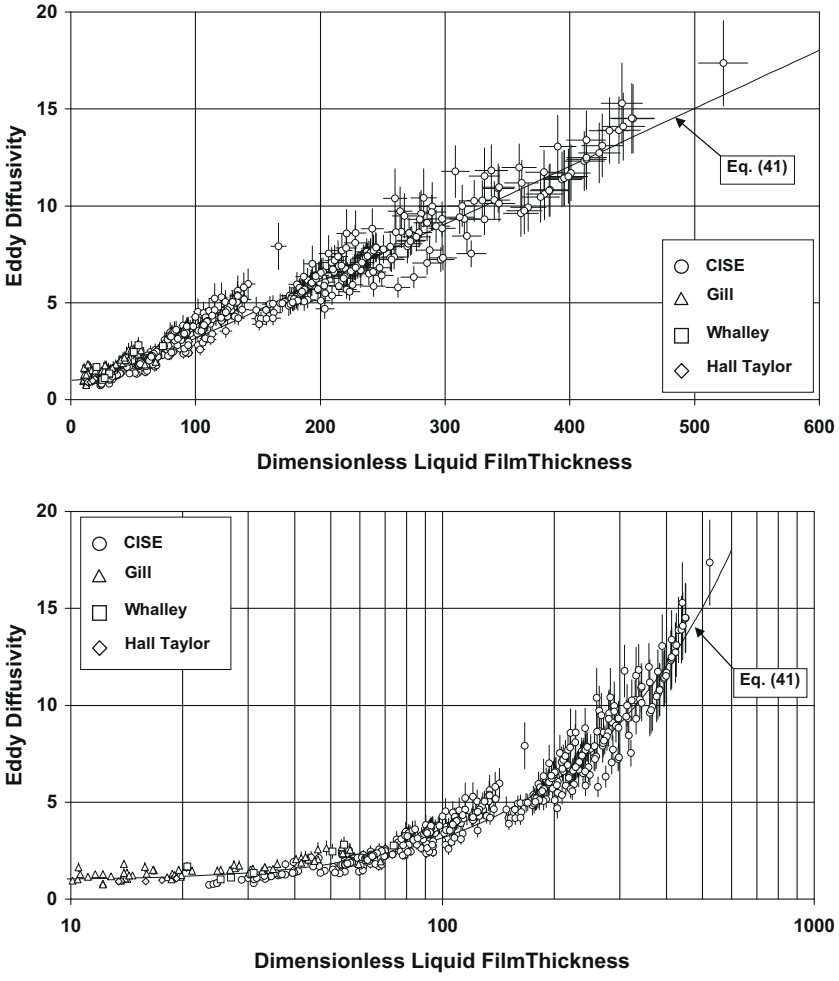

Fig. 5. Eddy diffusivity in the liquid film: x-axis linear scale (top) and logarithmic scale (bottom).

modeling with the gas phase moving faster than the liquid phase, the homogeneous void fraction provides an upper bound for the void fraction itself. As such, the comparison with the homogeneous model prediction can be regarded as a consistency check for the calculated annular flow void fraction. As seen in Fig. 2, the homogeneous model systematically overpredicts the calculated void fraction values, with an asymptotic tendency to become accurate in the limit of mist flow, where it should actually be applicable. The correlation due to Lockhart and Martinelli (1949) is one of the simplest void fraction correlations available and is representative of a family of simple correlations that relate the void fraction to the vapor quality and to the densities and viscosities of the phases (Butterworth, 1975). The correlation of Woldesemayat and Ghajar (2007), on the other hand, is based on the drift flux model originally proposed by Zuber and Findlay (1965) and is among the most accurate general purpose void fraction correlations currently available (Woldesemayat and Ghajar, 2007). The agreement between the calculated void fractions with those predicted by both correlations is good, as shown in Figs. 3 and 4.

The results regarding the eddy diffusivity in the liquid film are presented in Fig. 5, where the values calculated with Eq. (35) are displayed versus the dimensionless average liquid film thickness. It is worth noting that only the predictions of Eq. (35) with an uncertainty within ±15% are included in Fig. 5, corresponding to ~45% of the entire database. In order to properly capture both asymptotic trends for thin and thick films, the same plot is presented with both a linear (top) and a logarithmic (bottom) x-axis scale. All the calculated values for the eddy diffusivity cluster reasonably well, thus supporting the assumed dependence of the liquid film eddy diffusivity on the average liquid film thickness. In particular, with the exception of very thin liquid films, the trend in the data in Fig. 5 suggests a linear dependence of the eddy diffusivity on the dimensionless average liquid film thickness. In fluid-bounded flows, such as jets or mixing layers, the eddy diffusivity typically scales linearly with the local thickness of the bounded flow. The linear asymptotic trend that emerges in Fig. 5, therefore, actually provides further support to the turbulence modeling philosophy proposed in the present study for the liquid film. Furthermore, in Fig. 5, the eddy diffusivity properly approaches unity in the limit of thin films, suggesting that turbulence is gradually damped out as the liquid film becomes thinner and thinner. The scatter in the data, however, prevents locating the threshold for the liquid film thickness below which laminarization of the flow occurs. Besides, from inspection of Fig. 5, a mild discontinuity in the eddy diffusivity trend can be noticed for a dimensionless liquid film thickness value of ~150. The uncertainty of the calculated eddy diffusivity values, however, is too large to properly resolve the trend, and a more accurate experimental database would be necessary. The liquid film eddy diffusivity, in the limits of the present study, is well represented by the following

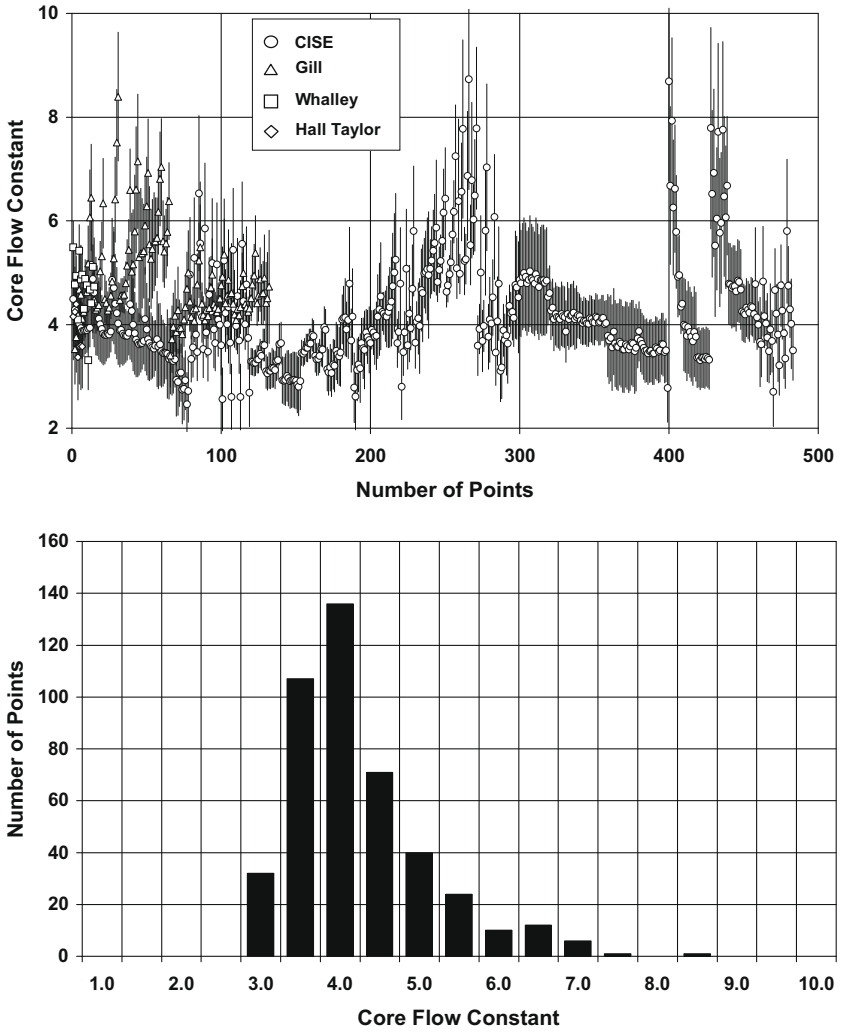

Fig. 6. Core flow constant a: calculated values (top) and histogram (bottom).

Eq. (41), which can be fed into Eq. (31) to provide the velocity profile for the liquid film:

$$\in_{lf}^{+} = \sqrt{1 + 0.9 \times 10^{-3}(t^{+})^{2}} \tag{41}$$

In summary, the proposed correlation is asymptotically consistent with the trends observed in Fig. 5 and depends on just one empirical parameter.

The results regarding the core flow are presented in Fig. 6, where the values of parameter a calculated from Eq. (36) are displayed (top) together with the histogram of the calculated values (bottom). It is worth noting that only the predictions from Eq. (36) with an uncertainty within ±25% are included in Fig. 6, corresponding to ∼45% of the entire database. Within the limits of the present study, the parameter a was not found to show any appreciable dependence on any flow parameter. As seen in Fig. 6, however, the uncertainty of the calculated values of the parameter a is large enough to hide any fine detail in the data. The average value of parameter a in Fig. 6 is 4.2 ± 1.0, with a standard deviation of ∼24%. In order to put this result into perspective, it is useful to recall the logarithmic law of the wall for single-phase wall-bounded flows, Eq. (42), which yields the velocity profile in the boundary layer not too close to the wall:

$$V^{+} = A\ln(y^{+}) + B, \quad y^{+} \geq 30 \tag{42}$$

The constants A and B are derived empirically, and the most frequently used values are $A = 2.5$ and $B = 5.5$ (Kakaç et al., 1987). Zanoun et al. (2003) provide a collection of values proposed for the constants A and B by different researchers in the last few decades. If all such values are averaged out one gets $A = 2.6 \pm 0.2$ and $B = 5.5 \pm 0.7$, so that the standard deviations are ∼8% and ∼14%, respectively. In this perspective, therefore, the standard deviation of ∼24% found for the parameter a in the present study appears to be encouraging. As already pointed out, the simple linear dependence of the core flow eddy diffusivity on the dimensionless distance from the wall, Eq. (30), is a first approximation that may require refinement in the future should a more accurate experimental database become available.

4. Results

As already pointed out, the mass flow rate of the liquid film can be calculated by integrating the liquid film velocity profile, as indicated in Eq. (33). In particular, if the velocity profile is provided by Eq. (31), together with Eq. (41) for the turbulence model, then Eq. (33) can be numerically solved for the average liquid film thickness. The calculated average liquid film thickness can then be compared with the measured value included in the data bank to provide a check for the liquid film velocity profile, as shown in Fig. 7. It is worth noting that only the predictions with an uncertainty within ±10% are included in Fig. 7, corresponding to ∼44% of the entire database. As can be seen, the comparison is satisfactory, showing that the calibration of the liquid film turbulence model was correctly carried out. Besides the velocity profile proposed in the present study, Eqs. (31) and (41), other velocity profiles can be used for the liquid film to calculate its average thickness with Eq. (33). In the present study, in particular, both the universal velocity profile for single-phase wall-bounded flow and the two-layer velocity profile of Dobran (1983) are used. Several different empirical representations are available for the universal velocity profile (Kakaç et al., 1987), with the discrepancy among the different representations being of the same order as the scatter in the available experimental data. As such, the choice of a particular representation is a question of personal choice and convenience. Here, the following representation due to von Karman (Kakaç et al., 1987) is used:

$$V^{+} = y^{+}, \quad 0 \leq y^{+} \leq 5 \tag{43}$$

$$V^{+} = 5.0\ln(y^{+}) - 3.05, \quad 5 \leq y^{+} \leq 30 \tag{44}$$

$$V^{+} = 2.5\ln(y^{+}) + 5.5, \quad y^{+} \geq 30 \tag{45}$$

In the context of the two-layer model of Dobran (1983), the dimensionless thickness of the continuous liquid base layer in contact with the channel wall t_{base}^{+} is estimated as follows:

$$t_{base}^{+} = 140 d^{+} Gr_{D}^{0.433} Re_{D}^{-1.35}, \quad 1.5 \times 10^{4} \leq Re_{D} \leq 1.5 \times 10^{5} \tag{46}$$

where the two-phase Grashoff number Gr_D and the core flow Reynolds number Re_D are defined as follows:

$$Gr_{D} = \left[\frac{g d^{3} \rho_{l}(\rho_{l} - \rho_{g})}{\mu_{l}^{2}}\right]^{0.5}; \quad Re_{D} = \frac{\rho_{c} J_{g} d}{\mu_{g}} \tag{47}$$

According to Dobran (1983), the velocity profile is provided by Eqs. (43)–(45) within the continuous liquid base layer, i.e. for $y^{+} < t_{base}^{+}$ while the following expression is used for the wavy liquid layer:

$$V^{+} = V^{+}(t_{base}^{+}) + \frac{y^{+} - t_{base}^{+}}{1 + 1.6 \times 10^{-3}(t^{+} - t_{base}^{+})^{1.8}}\left[1 - \left(1 - \frac{\tau_{i}}{\tau_{w}}\right)\frac{y^{+} + t_{base}^{+}}{2t^{+}}\right] \quad y^{+} \geq t_{base}^{+} \tag{48}$$

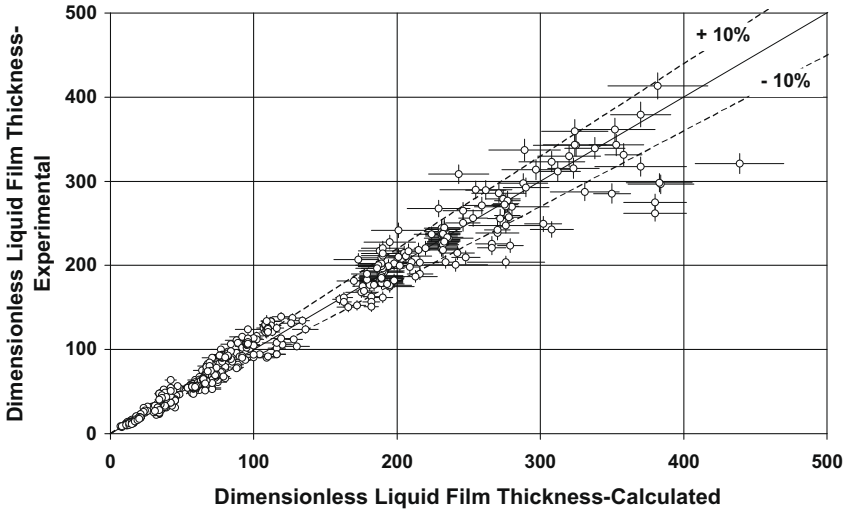

Fig. 7. Average liquid film thickness: experimental vs. reconstructed with Eqs. (31) and (41).

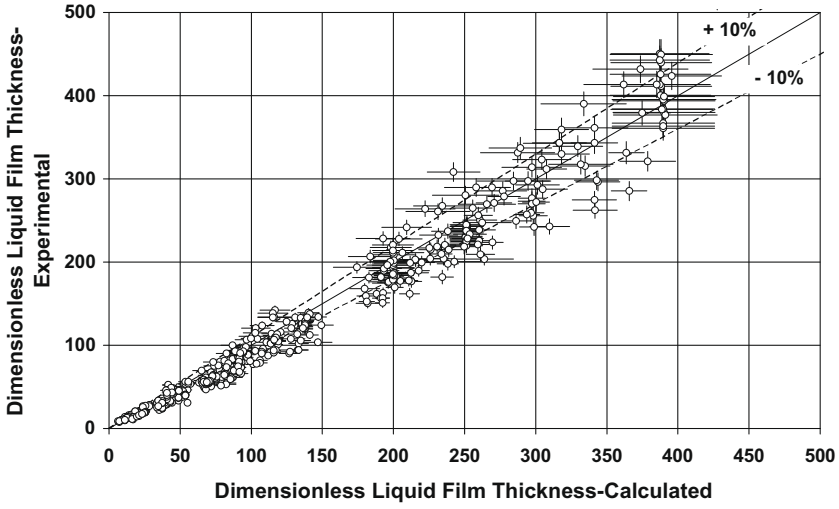

Fig. 8. Average liquid film thickness: experimental vs. reconstructed with universal velocity profile, Eqs. (43)–(45).

The velocity at the edge of the continuous liquid base layer $V^+(t^+_{base})$ is calculated with the universal velocity profile, Eqs. (43)–(45), while the interfacial shear stress τ_i is estimated from the conservation of linear momentum for the liquid film as follows:

$$\tau_i = \frac{(1-x)G}{\rho_l(1-\varepsilon)} G_e \left(\frac{1-e}{1-\gamma} - \frac{e}{\gamma}\right) + \frac{R}{R-t}\tau_w - \frac{R^2}{2(R-t)}(1-\varepsilon)(1-\gamma)\left(\frac{|\Delta P_{tot}|}{L_{dp}} - \rho_l g \sin\theta\right) \tag{49}$$

where G_e is the rate of liquid entrainment. The first term on the right-hand side of Eq. (49) accounts for the exchange of momentum from the gas core to the liquid film related to the different velocities the droplets have during entrainment and deposition. This term, within the limits of the present study, is a correction typically an order of magnitude smaller than the other two terms on the right-hand side of Eq. (49), so that the final result for the interfacial shear stress is not that sensible to the correlation that is selected to estimate the rate of entrainment G_e. Here, in particular, the following empirical correlation proposed by Kataoka et al. (2000) is used:

$$\frac{G_e d}{\mu_l} = 0.022 Re_K^{0.74} \left(\frac{\mu_g}{\mu_l}\right)^{0.26} E_\infty^{0.74} \tag{50}$$

The variables appearing in Eq. (50) are defined as follows:

$$Re_K = \frac{\rho_l J_l d}{\mu_l}; \quad E_\infty = \tanh\left(7.25 \times 10^{-7} We_K^{1.25} Re_K^{0.25}\right);$$
$$We_K = \frac{\rho_g J_g^2 d}{\sigma}\left(\frac{\rho_l - \rho_g}{\rho_g}\right)^{\frac{1}{3}} \tag{51}$$

The comparison between the measured average liquid film thicknesses and the calculated values using the universal velocity profile and the two-layer velocity profile of Dobran are presented in Figs. 8 and 9, respectively. It is worth noting that only the predictions with an uncertainty within ±10% are included in Figs. 8 and 9, corresponding to ~45% and ~61% of the entire database for the universal velocity profile and the two-layer velocity profile of Dobran, respectively. As can be seen, the universal velocity profile allows a reasonably accurate estimate of the average liquid film thickness, while the two-layer model of Dobran yields a significant overprediction. Actually, from inspection of Fig. 9 it can be seen that the two-layer model of Dobran works properly only for very thin films, as might be expected since the experimental data used by Dobran to calibrate the model are limited to thin liquid films. Recalibration of a two-layer model to extend its

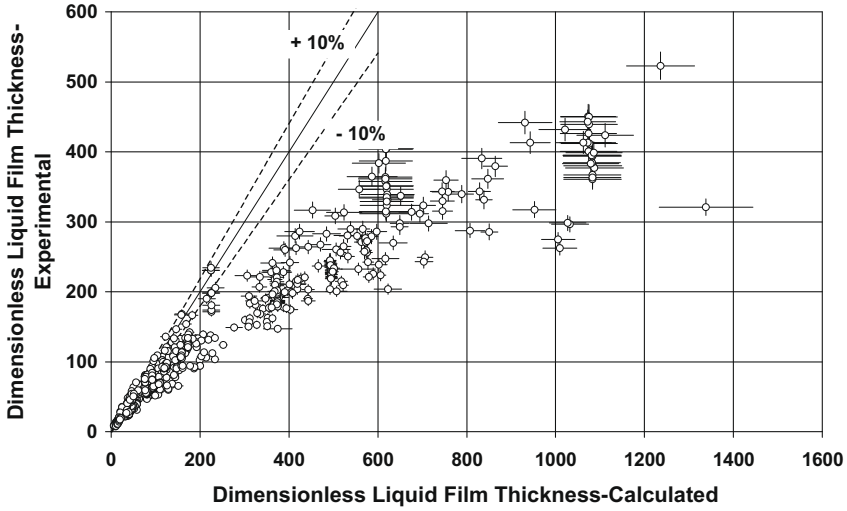

Fig. 9. Average liquid film thickness: experimental vs. reconstructed with Dobran velocity profile, Eq. (48).

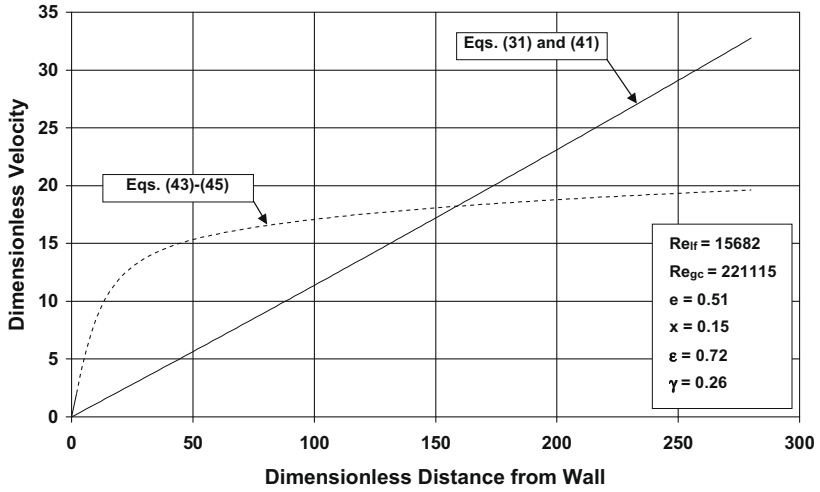

Fig. 10. Liquid film velocity profile comparison.

validity, as already discussed in the Introduction, is not straightforward. Fig. 10 reports the liquid film velocity profile as predicted with both the model presented in this study, Eqs. (31) and (41), and with the universal velocity profile, Eqs. (43)–(45). The two models assume different turbulence structures within the liquid film, and this is reflected by the different shapes of the predicted velocity profiles. The area underlying the two velocity profiles, however, is not that different, and this explains the relatively good performance of the universal velocity profile in predicting the average liquid film thickness.

CISE researchers (Silvestri et al., 1963) additionally performed local measurements of the core flow velocity. A comparison between the measured core flow velocities and the velocity profiles predicted with Eq. (32), using the core flow parameter $a = 4.2$, is provided in Figs. 11–13. In Fig. 14, finally, the experimental and predicted local gas core velocities are compared. It is worth noting that such data regarding the core flow velocity were not used in the calibration of the turbulence models. The comparisons can be considered satisfactory from inspection of Figs. 11–14 and, in particular, a systematic tendency of the proposed core flow velocity profile to overpredict close to the liquid film interface and to underpredict close to the center of the channel can be noticed. Among the several simplifying assumptions made to derive Eq. (32) that might be responsible for this tendency, the assumption regarding the distribution of the entrained liquid droplets is believed to play a major role. In the annular flow model described in Section 2, both the density and viscosity of the core flow have been calculated on a homogeneous core flow basis, Eqs. (14) and (27). Implicit in this approach is assuming that the entrained liquid droplets are uniformly distributed throughout the core flow area. Existing evidence (Levy, 1999), however, reveals that the entrained droplets can be far from being uniformly distributed. Typically, higher droplet concentrations are found close to the liquid film, where the droplets are continually generated, while lower droplet concentrations are found in the central part of the channel. Since the higher the local entrained droplets loading the lower the local velocity, assuming a uniform droplet concentration in the core cross section is likely to yield overprediction of the velocity close to the liquid film and underprediction close to the channel axis, as it is actually observed in the present study.

As already pointed out, the conservation of linear momentum for the total flow relates the wall shear stress τ_w to the total pressure gradient $(\Delta P_{tot}/L_{dp})$, as indicated in Eq. (13). On the other hand, the definition of the Fanning friction factor f relates the wall shear stress τ_w to the mean value of the dimensionless velocity profile in the liquid film $(V_{lf}^{+})_{avg}$ and in the gas core $(V_{gc}^{\sim})_{avg}$ as follows:

$$f = \frac{\tau_w}{\frac{1}{2}\rho V^2} = \frac{2}{(V_{lf}^{+})_{avg}^2} = \frac{2}{(V_{gc}^{\sim})_{avg}^2} \tag{52}$$

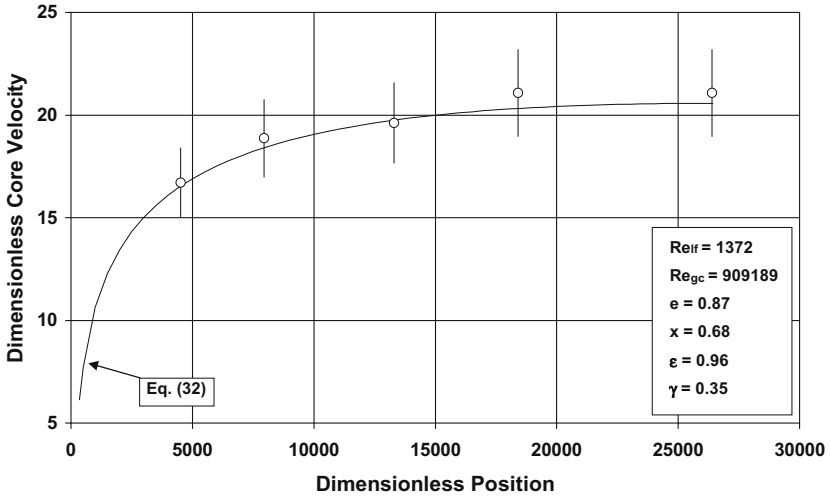

Fig. 11. Core flow velocity profile: measured local values vs. predicted profile.

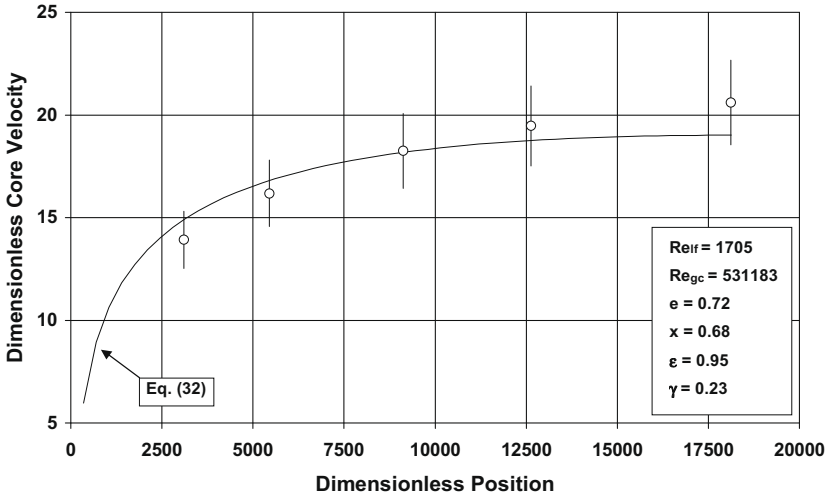

Fig. 12. Core flow velocity profile: measured local values vs. predicted profile.

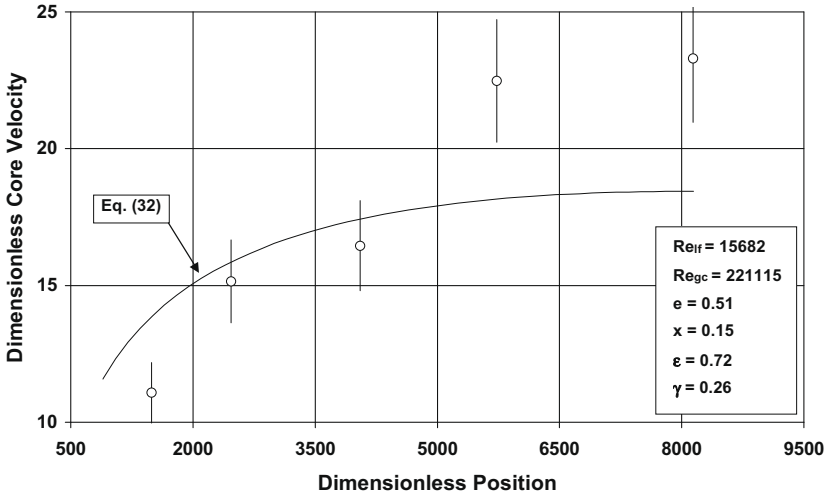

Fig. 13. Core flow velocity profile: measured local values vs. predicted profile.

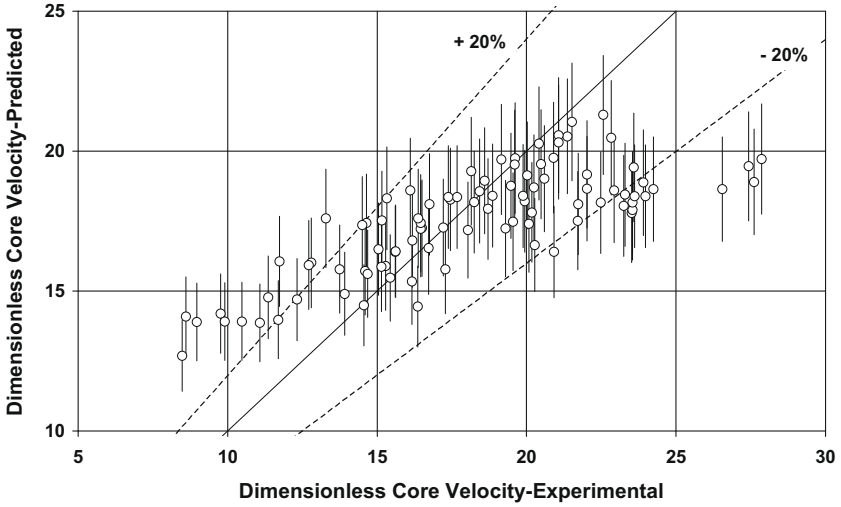

Fig. 14. Core flow velocity: predicted vs. experimental.

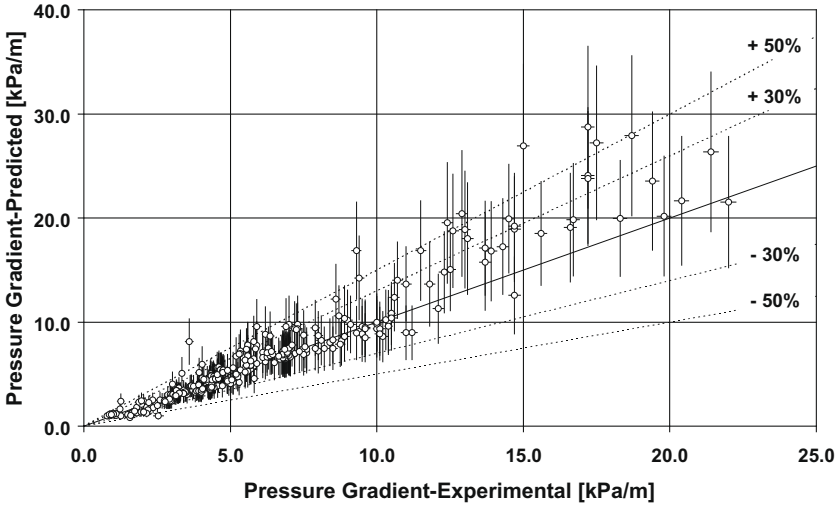

Fig. 15. Pressure gradient: predicted with Eq. (53) vs. experimental.

where ρ is the fluid density and V is the average velocity. Combining Eqs. (13) and (52) and rearranging yields two relationships that allow the calculation of the pressure gradient as follows:

$$\left(\frac{\Delta P_{tot}}{L_{dp}}\right) = \frac{1}{1-\xi}\left[\frac{2G_{lf}^2}{R\rho_l (V_{lf}^+)_{avg}^2} + \rho_{mix} g \sin\theta\right] \tag{53}$$

$$\left(\frac{\Delta P_{tot}}{L_{dp}}\right) = \frac{1}{1-\xi}\left[\frac{2G_{gc}^2}{R\rho_c (V_{gc}^{\sim})_{avg}^2} + \rho_{mix} g \sin\theta\right] \tag{54}$$

where G_{lf} and G_{gc} are the liquid film and the droplet laden gas core mass fluxes, respectively. The mean values of the velocity profile in the liquid film $(V_{lf}^+)_{avg}$ and in the gas core $(V_{gc}^{\sim})_{avg}$ can be calculated by integrating the respective velocity profiles, Eqs. (31) and (32), as follows:

$$(V_{lf}^+)_{avg} = \frac{2}{t^+(2R^+ - t^+)\in_{lf}^+}\left(\frac{I_1}{1-\xi} + \frac{1}{2}C_{lf} I_2\right) \tag{55}$$

$$\left(V_{gc}^{\sim}\right)_{avg} = \sqrt{\frac{\rho_c}{\rho_l}} V_{lf}^+(t^+) + \frac{2a}{(R^{\sim} - t^{\sim})^2}\left(\frac{1}{1-\xi} + C_{gc} R^{\sim}\right)\left(I_3 - \frac{I_4}{R^{\sim}}\right) \tag{56}$$

The parameters I_1–I_4 appearing in Eqs. (55) and (56) are defined as follows:

$$I_1 = \frac{(t^+)^4}{8R^+} - \frac{(t^+)^3}{2} + \frac{R^+(t^+)^2}{2} + \frac{\xi(R^+)^3}{2} \times \left\{-\frac{1}{2} + \left(1 - \frac{t^+}{R^+}\right)^2\left[\frac{1}{2} - \ln\left(1 - \frac{t^+}{R^+}\right)\right]\right\} \tag{57}$$

$$I_2 = \frac{R^+(t^+)^3}{3} - \frac{(t^+)^4}{4} \tag{58}$$

$$I_3 = \frac{1}{2}(R^{\sim})^2 \ln\left(\frac{R^{\sim}}{t^{\sim}}\right) - \frac{3}{4}(R^{\sim})^2 + R^{\sim} t^{\sim} - \frac{1}{4}(t^{\sim})^2 \tag{59}$$

$$I_4 = \frac{1}{6}(R^{\sim} - t^{\sim})^3 \tag{60}$$

The comparison between the measured pressure gradients and the values calculated with Eqs. (53) and (54) is presented in Figs. 15 and 16, respectively, while the statistical comparison between measurements and predictions is reported in Table 4. It is worth noting that only the pressure gradient predictions from Eqs. (53) and (54) with an uncertainty within ± 30% are included in Figs. 15 and 16, corresponding to ~29% and ~70% of the entire database for Eqs. (53) and

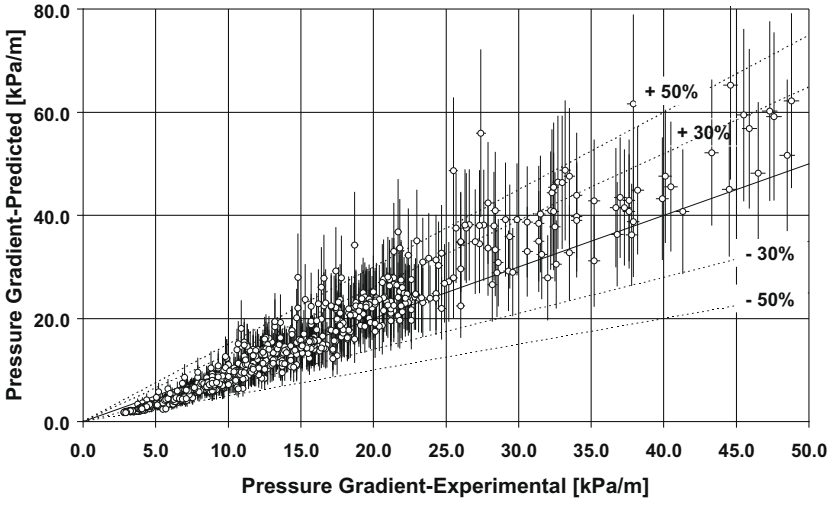

Fig. 16. Pressure gradient: predicted with Eq. (54) vs. experimental.

Table 4
Pressure gradient: statistical comparison between measurements and predictions.

	(1)	(2)	(3)	(4)
Liquid film, Eq. (53)	14.0	−3.6	88.3	96.9
Gas core, Eq. (54)	22.0	9.3	68.9	98.1

(1) Mean deviation (%) $\frac{100}{n}\sum_1^n \frac{\left|\left(\Delta P_{tot}/L_{dp}\right)_{exp}-\left(\Delta P_{tot}/L_{dp}\right)_{cal}\right|}{\left(\Delta P_{tot}/L_{dp}\right)_{exp}}$.

(2) Average deviation (%) $\frac{100}{n}\sum_1^n \frac{\left(\Delta P_{tot}/L_{dp}\right)_{exp}-\left(\Delta P_{tot}/L_{dp}\right)_{cal}}{\left(\Delta P_{tot}/L_{dp}\right)_{exp}}$.

(3) Percentage of experimental data within ±30%.

(4) Percentage of experimental data within ±50%.

Table 5
Limits of applicability of the proposed turbulence models.

Re_{lf}	1×10^2–3×10^4
Re_{gc}*	3×10^4–1×10^6
e	0.05–0.98
x	0.06–0.97
ε	0.52–0.99

* Gas core Reynolds number: $Re_{gc}=\frac{4}{\pi}\frac{\Gamma_g+e\Gamma_l}{(d-2t)\mu_c}$.

(54), respectively. Besides, for thin liquid films the pressure gradient estimate from Eq. (53) becomes highly inaccurate. As such, the pressure gradient estimate from Eq. (53) is of practical use for a subset of the experimental database only, and the pressure gradient estimate from Eq. (54) is therefore of more general applicability. As can be seen in Figs. 15 and 16 and Table 4, the agreement between measurements and predictions is quite satisfactory, showing that the calibration of the turbulence models was correctly carried out.

The applicability of the newly proposed turbulence models is limited to the range of parameters summarized in Table 5.

5. Conclusions

New algebraic turbulence models are proposed for both the liquid film and the droplet laden gas core of adiabatic gas–liquid annular two-phase flow. Both turbulence models are limited to turbulent momentum transport and are calibrated with a database collected from the open literature. Special care is taken in keeping the turbulence models simple to minimize the number of empirical tuning parameters. The amount of experimental information required for the calibration of the turbulence models is limited to a few, easily accessible flow parameters, together with the one-dimensional annular flow model presented. The fraction of liquid entrained as droplets in the gas core is empirically estimated. This highlights the dependence of the results presented on this key parameter of annular two-phase flow.

The proposed turbulence models reproduce the key parameters of annular flow well (average liquid film thickness and pressure gradient), showing that their calibration was correctly carried out and providing support for the algebraic turbulence modeling assumptions made.

The proposed velocity profile for the annular liquid film reproduces the average liquid film thickness better than both the universal velocity profile borrowed from single-phase flow theory and the more sophisticated two-layer annular film model of Dobran (1983).

The proposed algebraic turbulence model for the droplet-laden gas core predicts realistic velocity profiles that compare favorably with available measurements of the core flow velocity. Nonetheless, the proposed turbulence model for the core flow is still preliminary and should be finalized with a more detailed and accurate experimental database.

Although limited to turbulent momentum transport, the proposed turbulence models can be used as a starting point for more sophisticated modeling of annular flow, specifically for annular flow heat transfer in diabatic flows.

Acknowledgement

A. Cioncolini is supported by Swiss National Fund (SNF) Contract No. 200020-119651.

Appendix A

A force balance on a liquid film slice extending from the tube wall ($r = R$) to a position r yields:

$$\tau_{lf}(r)=\frac{R}{r}\tau_w+\frac{R^2-r^2}{2r}\left(\frac{dP}{dz}+\rho_l g\sin\theta\right),\quad (R-t)\le r\le R \tag{A1}$$

The conservation of the linear momentum for the total flow yields:

$$\frac{x^2G^2}{\varepsilon}\frac{dv_g}{dz}=-\frac{dP}{dz}-\frac{2\tau_w}{R}-\rho_{mix}g\sin\theta \tag{A2}$$

The accelerative term appearing on the right-hand side of Eq. (A2) can be expressed as follows:

$$\frac{x^2G^2}{\varepsilon}\frac{dv_g}{dz}=-\frac{x^2G^2}{\varepsilon}\left|\frac{dv_g}{dP}\right|\frac{dP}{dz}=-\xi\frac{dP}{dz};\quad \xi=\frac{x^2G^2}{\varepsilon}\left|\frac{dv_g}{dP}\right| \tag{A3}$$

Substitution of Eq. (A3) into Eq. (A2) yields:

$$(1-\xi)\frac{dP}{dz}=-\frac{2\tau_w}{R}-\rho_{mix}g\sin\theta \tag{A4}$$

Using Eq. (A4) to eliminate the pressure gradient from Eq. (A1) yields:

$$\tau_{lf}(r)=\frac{1}{1-\xi}\left(\frac{r}{R}-\xi\frac{R}{r}\right)\tau_w+\frac{R^2-r^2}{2r}\left(\rho_l-\frac{\rho_{mix}}{1-\xi}\right)g\sin\theta,\quad (R-t)\le r\le R \tag{A5}$$

Switching from the radial coordinate r to the distance from the tube wall y yields:

$$\tau_{lf}(y)=\frac{1}{1-\xi}\left(1-\frac{y}{R}-\xi\frac{R}{R-y}\right)\tau_w+\frac{y(2R-y)}{2(R-y)}\left(\rho_l-\frac{\rho_{mix}}{1-\xi}\right)g\sin\theta,\quad 0\le y\le t \tag{A6}$$

A force balance on a core flow slice extending from the tube axis ($r = 0$) to a position r yields:

$$\tau_{gc}(r)=-\frac{r}{2}\left(\frac{dP}{dz}+\rho_c g\sin\theta\right),\quad 0\le r\le (R-t) \tag{A7}$$

Using Eq. (A4) to eliminate the pressure gradient from Eq. (A7) yields:

$$\tau_{gc}(r)=\frac{1}{1-\xi}\frac{r}{R}\tau_w+\frac{r}{2}\left(\frac{\rho_{mix}}{1-\xi}-\rho_c\right)g\sin\theta \tag{A8}$$

Switching from the radial coordinate r to the distance from the tube wall y yields:

$$\tau_{gc}(y)=\frac{1}{1-\xi}\left(1-\frac{y}{R}\right)\tau_w+\frac{1}{2}(R-y)\left(\frac{\rho_{mix}}{1-\xi}-\rho_c\right)g\sin\theta,\quad t\le y\le R \tag{A9}$$

Eqs. A6 and A9 are included in the paper as Eqs. (4) and (5).

Appendix B

Block-diagram illustrating the implementation of the annular flow model calculations:

Block-diagram illustrating the implementation of the annular flow model calculations:

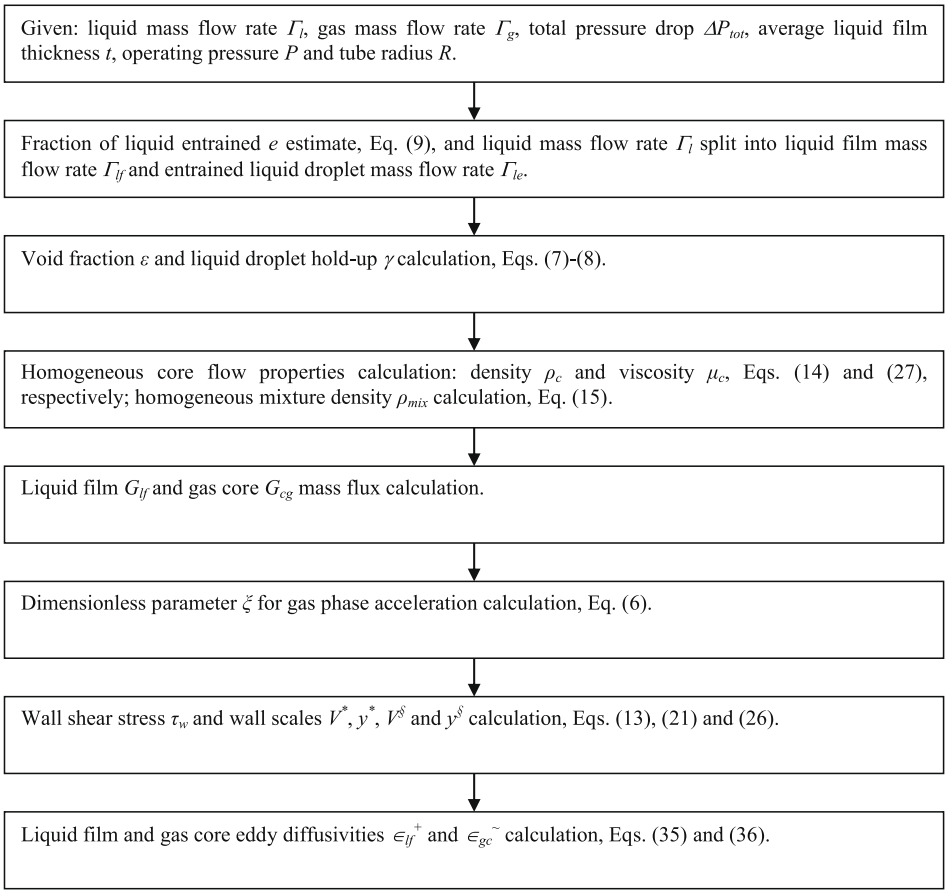

References

Abolfald, M., Wallis, G.B., 1986. An improved mixing-length model for annular two-phase flow with liquid entrainment. Nucl. Eng. Des. 95, 233–241.

Adorni, N., Casagrande, I., Cravarolo, L., Hassid, A., Pedrocchi, E., Silvestri, M., 1963. Further investigations in adiabatic dispersed flow: pressure drop and film thickness measurements with different channel geometries-analysis of the influence of geometrical and physical parameters. CISE Report R-53.

Anderson, G.H., Mantzouranis, B.G., 1960. Two-phase (gas–liquid) flow phenomena-I: pressure drop and hold-up for two-phase flow in vertical tubes. Chem. Eng. Sci. 12, 109–126.

Azzopardi, B.J., 1997. Drops in annular two-phase flow. Int. J. Multiphase Flow 23, 1–53.

Azzopardi, B.J., 1999. Turbulence modification in annular gas–liquid flow. Int. J. Multiphase Flow 25, 945–955.

Bellinghausen, R., Renz, U., 1992. Heat transfer and film thickness during condensation of steam flowing at high velocity in a vertical pipe. Int. J. Heat Mass Transfer 35, 683–689.

Bradshaw, P., 1997. Understanding and prediction of turbulent flow-1996. Int. J. Heat Fluid Flow 18, 45–54.

Butterworth, D., 1974. An analysis of film flow and its application to condensation in a horizontal tube. Int. J. Multiphase Flow 1, 671–682.

Butterworth, D., 1975. A comparison of some void-fraction relationships for co-current gas–liquid flow. Int. J. Multiphase Flow 1, 845–850.

Casagrande, I., Cravarolo, L., Hassid, A., Pedrocchi, E., 1963. Adiabatic dispersed two-phase flow: further results on the influence of physical properties on pressure drop and film thickness. CISE Report R-73.

Cravarolo, L., Hassid, A., Pedrocchi, E., 1964. Further investigation on two-phase adiabatic annular-dispersed flow: effect of length and some inlet conditions on flow parameters. CISE Report R-93.

Dobran, F., 1983. Hydrodynamic and heat transfer analysis of two-phase annular flow with a new liquid film model of turbulence. Int. J. Heat Mass Transfer 26, 1159–1171.

Fore, L.B., Dukler, A.E., 1995. The distribution of drop size and velocity in gas–liquid annular flow. Int. J. Multiphase Flow 21, 137–149.

Gill, L.E., Hewitt, G.F., Lacey, P.M.C., 1964. Sampling probe studies of the gas core in annular two-phase flow-II: studies of the effect of phase flow rates on phase and velocity distribution. Chem. Eng. Sci. 19, 665–682.

Gill, L.E., Hewitt, G.F., Lacey, P.M.C., 1965. Data on the upwards annular flow of air–water mixtures. Chem. Eng. Sci. 20, 71–88.

Hall-Taylor, N., Hewitt, G.F., Lacey, P.M.C., 1963. The motion and frequency of large disturbance waves in annular two-phase flow of air–water mixtures. Chem. Eng. Sci. 18, 537–552.

Hewitt, G.F., Lacey, P.M.C., 1965. The breakdown of the liquid film in annular two-phase flow. Int. J. Heat Mass Transfer 8, 781–791.

Hewitt, G.F., 1998. Boiling. In: Rohsenow, W.M., Hartnett, J.P., Cho, Y.I. (Eds.), Handbook of Heat Transfer. McGraw-Hill, Boston.

Jayanti, S., Hewitt, G.F., 1997. Hydrodynamics and heat transfer in wavy annular gas–liquid flow: a computational fluid dynamics study. Int. J. Heat Mass Transfer 40, 2445–2460.

Jensen, M.K., 1987. The liquid film and the core region velocity profiles in annular two-phase flow. Int. J. Multiphase Flow 13, 615–628.

Kaji, M., Sawai, T., Mori, K., Yamauchi, S., Nakanishi, S., 1999. Numerical calculation of forced convection heat transfer to annular two-phase flow in an evaporating tube. In: Celata, G.P., Di Marco, P., Shah, R.K. (Eds.), Two-Phase Flow Modeling and Experimentation. ETS, Pisa, pp. 263–270.

Kakaç, S., Shah, R., Aung, W., 1987. Handbook of Single-Phase Convective Heat Transfer. Wiley, New York.

Kataoka, I., Ishii, M., Nakayama, A., 2000. Entrainment and deposition rates of droplets in annular two-phase flow. Int. J. Heat Mass Transfer 43, 1573–1589.

Kishore, B.N., Jayanti, S., 2004. A multidimensional model for annular gas–liquid flow. Chem. Eng. Sci. 59, 3577–3589.

Kumar, R., Trabold, T.A., 2000. High pressure annular two-phase flow in narrow ducts: part II – three-field modeling. ASME J. Fluids Eng. 122, 375–384.

Levy, S., 1966. Prediction of two-phase annular flow with liquid entrainment. Int. J. Heat Mass Transfer 9, 171–188.

Levy, S., Healzer, J.M., 1981. Application of mixing length theory to wavy turbulent liquid–gas interface. ASME J. Heat Transfer 103, 492–500.

Levy, S., 1999. Two-Phase Flow in Complex Systems. Wiley, New York.

Lockhart, R.W., Martinelli, R.C., 1949. Proposed correlation of data for isothermal two-phase, two-component flow in pipes. Chem. Eng. Prog. 45, 39–48.

Malamatenios, C., Giannakoglou, K.C., Papailiou, K.D., 1994. A coupled two-phase shear layer/liquid film calculation method: formulation of the problem and solution algorithm. Int. J. Multiphase Flow 20, 593–612.

Marchioli, C. et al., 2008. Statistics of particle dispersion in direct numerical simulations of wall bounded turbulence: results of an international collaborative benchmark test. Int. J. Multiphase Flow 34, 879–893.

Moeck, E.O., Stachiewicz, J.W., 1972. A droplet interchange model for annular-dispersed two-phase flow. Int. J. Heat Mass Transfer 15, 637–653.

Oliemans, R.V.A., Pots, B.F.M., Trompé, N., 1986. Modeling of annular dispersed two-phase flow in vertical pipes. Int. J. Multiphase Flow 12, 711–732.
Peng, S.W., 2008. Heat flux effect on the droplet entrainment and deposition in annular flow dryout. Commun. Nonlinear Sci. Numer. Simul. 13, 2223–2235.
Pu, F., Sui-Zheng, Q., Dou-Nan, J., 2006. An investigation of flow characteristics and critical heat flux in vertical upward round tube. Nucl. Sci. Tech. 17, 170–176.
REFPROP: Reference Fluid Thermodynamic and Transport Properties, 2007. NIST Standard Reference Database 23, Version 8.0.
Saito, T., Hughes, E.D., Carbon, M.W., 1978. Multi-fluid modeling of annular two-phase flow. Nucl. Eng. Des. 50, 225–271.
Schmitt, F.G., 2007. About Boussinesq's turbulent viscosity hypothesis: historical remarks and a direct evaluation of its validity. C.R. Mecanique 335, 617–627.
Shearer, C.J., Nedderman, R.M., 1965. Pressure gradient and liquid film thickness in co-current upwards flow of gas/liquid mixtures: application to film-cooler design. Chem. Eng. Sci. 20, 671–683.
Silvestri, M., Casagrande, I., Cravarolo, L., Hassid, A., Bertoletti, S., Lombardi, C., Peterlongo, G., Soldaini, G., Vella, G., Perona, G., Sesini, R., 1963. A research program in two-phase flow. CISE Report.
Tandon, T.N., Varma, H.K., Gupta, C.P., 1985. A void fraction model for annular two-phase flow. Int. J. Heat Mass Transfer 28, 191–198.
Tannehill, J.C., Anderson, D.A., Pletcher, R.H., 1997. Computational Fluid Mechanics and Heat Transfer. Taylor & Francis, Philadelphia.
Tong, L.S., Tang, Y.S., 1997. Boiling Heat Transfer and Two-Phase Flow. Taylor & Francis, Philadelphia.
Trabold, T.A., Kumar, R., 1999. Vapor core turbulence in annular two-phase flow. In: Celata, G.P., Di Marco, P., Shah, R.K. (Eds.), Two-Phase Flow Modeling and Experimentation. ETS, Pisa, pp. 1131–1139.
Ueda, T., Tanaka, T., 1974. Studies of liquid film flow in two-phase annular and annular-mist flow regions (part I: downflow in a vertical tube). Bull. JSME 17, 603–613.
Ueda, T., Nose, S., 1974. Studies of liquid film flow in two-phase annular and annular-mist flow regions (part II: upflow in a vertical tube). Bull. JSME 17, 614–624.
Vassallo, P., 1999. Near wall structure in vertical air–water annular flows. Int. J. Multiphase Flow 25, 459–476.
Whalley, P.B., Hewitt, G.F., Hutchinson, P., 1974. Institution of Chemical Engineering Symposium 38 (Multi-Phase Flow Systems).
Wilcox, D.C., 2002. Turbulence Modeling for CFD. DCW Industries, La Cañada.
Woldesemayat, M.A., Ghajar, A.J., 2007. Comparison of void fraction correlations for different flow patterns in horizontal and upward inclined pipes. Int. J. Multiphase Flow 33, 347–370.
Wolf, A., Jayanti, S., Hewitt, G.F., 2001. Flow development in vertical annular flow. Chem. Eng. Sci. 56, 3221–3235.
Zanoun, E.S., Durst, F., Nagib, H., 2003. Evaluating the law of the wall in two-dimensional fully developed turbulent channel flow. Phys. Fluids 15, 3079–3089.
Zuber, N., Findlay, J.A., 1965. Average volumetric concentration in two-phase flow systems. ASME J. Heat Transfer 87, 435–468.